Available online at www.sciencedirect.com
ScienceDirect
Trans. Nonferrous Met. Soc. China 26(2016) 974−983
Transactions of Nonferrous Metals Society of China
www.tnmsc.cn

Fracture energy evaluation on 7075-T651 aluminum alloy welds determined by instrumented impact pendulum

R. R. AMBRIZ[1], D. JARAMILLO[1], C. GARCÍA[2], F. F. CURIEL[3]

1. Instituto Politécnico Nacional CIITEC-IPN, Cerrada de Cecati S/N Col. Sta. Catarina C.P 02250, Azcapotzalco, DF, México;
2. Mechanical and Aerospace Engineering, Carleton University, 1125 Colonel By Drive, Ottawa, ON, K1S 5B6, Canada;
3. Universidad Autónoma de Coahuila (UAdeC), Facultad de Metalurgia, Carr. 57, Km 5, Monclova, Coahuila, México

Received 21 April 2015; accepted 10 October 2015

Abstract: By using an instrumented impact pendulum, the force versus time curves of 7075-T651 aluminum welds were obtained from standard Charpy-V samples. Considering the force−time curves and constant impact velocity, the fracture energies for different zones were quantified. A fracture energy improvement for the HAZ (33.6 J) was observed in comparison with the weld metal (7.88 J), and base metal (5.37 J and 7.37 J for longitudinal and transverse directions, respectively). This toughness increment was attributed to the microstructural transformation caused by the thermodynamic instability of η' precipitates during the welding. Fracture energy for weld metal was higher than that for base metal, probably due to pores created during solidification. Regarding the dynamic yielding force obtained from the force−time curves, an approximation to the dynamic yield strength for weld, HAZ and base metal was determined. Fracture surfaces revealed an intergranular failure for base metal in longitudinal direction, whereas a predominately brittle failure (cleavage) with some insights of ductile characteristics was observed for the transverse direction. In contrast, a ductile failure was observed for weld metal and HAZ.

Key words: 7075-T651 welded joint; instrumented Charpy pendulum; force−time curve; fracture energy; dynamic yield strength

1 Introduction

The 7075-T651 is an Al−Zn−Mg alloy with a high strength due to the temper treatment (artificial aging and cold forming), which provides a minimal tensile strength of 538 MPa [1]. The high strength in combination with the low density of the 7075-T651 aluminum alloy (2810 kg/m^3) produces a good specific strength, that is suitable for structures and components subjected to static and dynamic loads. Frequently, this alloy is welded by fusion processes. The thermal cycles imposed by the heat source during the welding provide heterogeneous mechanical properties in the joints [2−5]. For instance, a microstructural transformation takes place in the heat affected zone (HAZ), and tensile mechanical properties of the welded joint decrease considerably. HWANG and CHOU [6] studied the microstructural transformation and tensile mechanical properties of the HAZ in welds of a 7075-T651 aluminum alloy. They found that the decrease of the yield strength in the HAZ was due to the transformation of fine η' precipitates to coarse η precipitates, according to the following precipitation sequence [7]: Supersaturated solid solution (α_{sss})→ Guinier–Preston zones (GP)→η'→η, ALATORRE et al [5] determined the tensile mechanical properties and the fusion zone hardening in welds of a 7075-T651. They found that the tensile strength in gas metal arc welding (GMAW) decreased by more than 50% with respect to the base material. Also, different zones in the welded joints performed by GMAW and modified indirect electric (MIEA) welding techniques were identified by means of microhardness measurements (maps and profiles). In both welding techniques, a soft zone formation in the HAZ due to the microstructural transformation of η' to η precipitates was identified. This zone was symmetrically located at distances of 15 and 20 mm from the center of the welding bead for GMAW and MIEA, respectively.

TAJALLY et al [8] realized a comparative analysis

Corresponding author: R. R. AMBRIZ; Tel: +52-57-296000; Fax: +52-55-617536; E-mail: rrambriz@ipn.mx
DOI: 10.1016/S1003-6326(16)64157-2

of the tensile and the impact-toughness behavior of a 7075 aluminum alloy with cold rolled samples and different annealed temperatures. Impact toughness was determined using classical Charpy V-notch sub-size tests specimens. They found that cold working and annealing temperatures have an important effect on the impact toughness. For instance, the fracture energy of the starting material (7075-T0) decreased from 19.7 J to 10.4 J for the same material with a cold working of 60% and recrystallized at 350 °C.

The instrumented impact tester pendulum [9−11], and three-point bending tests have been used to determine the dynamic fracture behavior on aluminum alloys. An experimental study on the dynamic fracture of extruded 7xxx aluminum alloys was carried out by CHEN at al [9]. They used an instrumented Charpy pendulum to determine the total energy absorbed on 7003-T6 and 7108-T6 aluminum alloys.

This work reports the results obtained from instrumented Charpy tests in welds of a 7075-T651 aluminum alloy. The impact behavior of the base metal (longitudinal and transverse to rolling direction), HAZ and weld metal was evaluated in terms of the force versus time curves, the fracture energy and the fracture surfaces. A brittle behavior was identified for the base metal, while ductile characteristics were observed for the HAZ and the weld metal.

2 Experimental

The base material used was a 7075-T651 aluminum plate of 2400 mm × 1200 mm × 12.7 mm. The chemical compositions of the base and weld metals are shown in Table 1.

Table 1 Chemical compositions of materials used (mass fraction, %)

Material	Al	Si	Fe	Cu	Mn
7075-T651*	88.6	0.03	0.19	1.7	0.02
ER5356**	95.04	–	–	–	–
Material	Mg	Cr	Zn	Ti	Others
7075-T651*	2.7	0.18	6.4	0.02	0.16
ER5356**	4.96	–	–	–	–

* Optical emission spectrometry; ** Energy dispersive X-ray spectroscopy

A double-V joint preparation according to Fig. 1 was performed on plates of 300 mm × 150 mm × 9.0 mm. Welded joints were produced by gas metal arc welding (GMAW) process, by applying a welding speed of 3.6 mm/s, direct current electrode positive (DCEP) polarity, argon flow of 1.55 m^3/h, stick-out of 10 mm, voltage of 23 V, feeding speed of 110 mm/s, and current of 142 A.

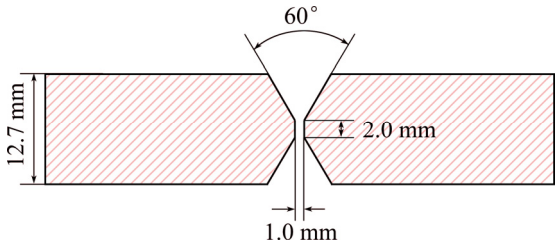

Fig. 1 Double-V joint preparation for GMAW

From the welded plates, standard Charpy V-notch samples were machined for the base metal (rolling and transverse directions), the weld metal and the HAZ according to the dimensions dictated in ASTM E23 standard. Four specimens were tested for each condition. Figure 2 shows the schematic representation for the Charpy V-notch in different zones of the welded joint.

The notch for the HAZ (soft zone) and weld metal specimens was located according to the microhardness profile shown in Fig. 3 [5].

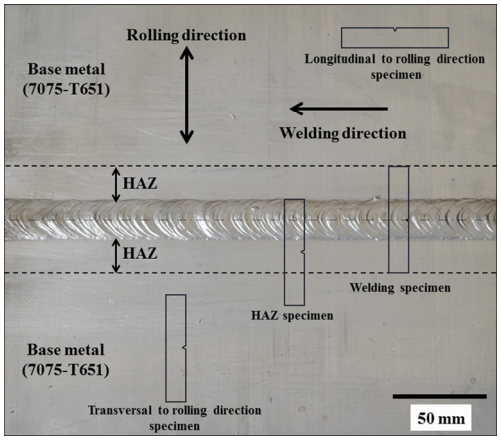

Fig. 2 Schematic representation of Charpy V-notch samples taken from welded plate

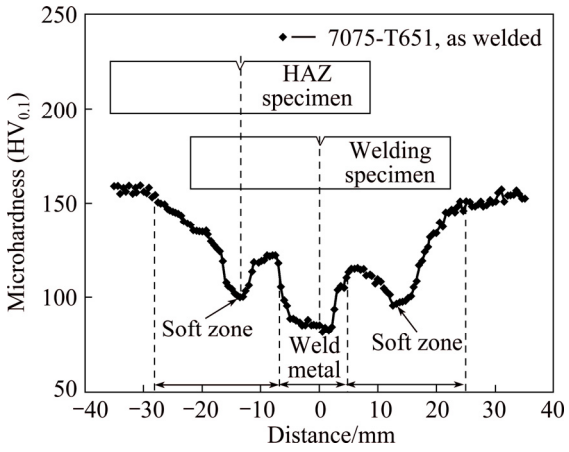

Fig. 3 Microhardness profile obtained for 7075-T651 aluminum alloy GMAW welds [5]

For the evaluation of the impact resistance, an instrumented Charpy pendulum with capacity of 258 J, and impact velocity of 5.24 m/s was used. Strain gages connected to a full Wheatstone bridge were used at striker as shown in Fig. 4.

The strain evolution of the striker was digitalized by a data acquisition system at the frequency of 100 kHz as recommended by the ASTM E2298 standard. Before the impact tests, the striker was calibrated in static conditions applying different forces with a hydraulic machine to obtain the force−strain evolution in elastic conditions (see Fig. 5).

The strain measurements were used to determine the impact force according to the linear fitting equation depicted from the data of Fig. 5. The time for the test was obtained directly from the frequency of the data adquisition system, and force−time curves were plotted for each material.

The energy at different stages of the force−time curves was determined by the following equation:

$$E_{all} = E_{in} + E_{stable} + E_{unstable} = v_0\int_0^{t_{in}} F(t)\mathrm{d}t + v_0\int_{t_{in}}^{t_{iu}} F(t)\mathrm{d}t + v_0\int_{t_{iu}}^{t_a} F(t)\mathrm{d}t \quad (1)$$

where E_{all} is the fracture energy, E_{in} is the energy required for the crack nucleation, E_{stable} and $E_{unstable}$ are the stable and unstable crack propagation energies, respectively, v_0 is the initial impact velocity, and $F(t)\mathrm{d}t$ is the force−time evolution during the impact.

3 Results and discussion

3.1 Force−time evolution

Figure 6 shows the force−time behavior in Charpy V-notch samples for the base metal (longitudinal and transverse directions), weld metal and HAZ for the 7075-T651 aluminum alloy. In all materials, load oscillations as a function of the time were observed. These oscillations are considered a combination of a quasi-static force corresponding to the bending specimen (first mode), and a dynamic force related to the vibration of the specimen around its equilibrium configuration [10]. The oscillations appear during the impact as a combination of the first and second symmetric specimen vibration modes with a predominance of the first mode [12].

The evolution of the force−time curves for the base metal in both directions exhibited brittle characteristics. The maximum force reached was around 10 kN followed by an abrupt fall in the force, i.e., evidence of unstable crack growth was not observed. The time to fracture was 0.2 and 0.3 ms for longitudinal and transverse directions, respectively. Instead, for the weld metal and the HAZ, the fracture time tends to increase considerably and a ductile behavior was observed. However, the maximum force applied by the hammer to the Charpy V-notch samples machined from the weld metal and the HAZ (Fig. 2) was significantly lower than that of the

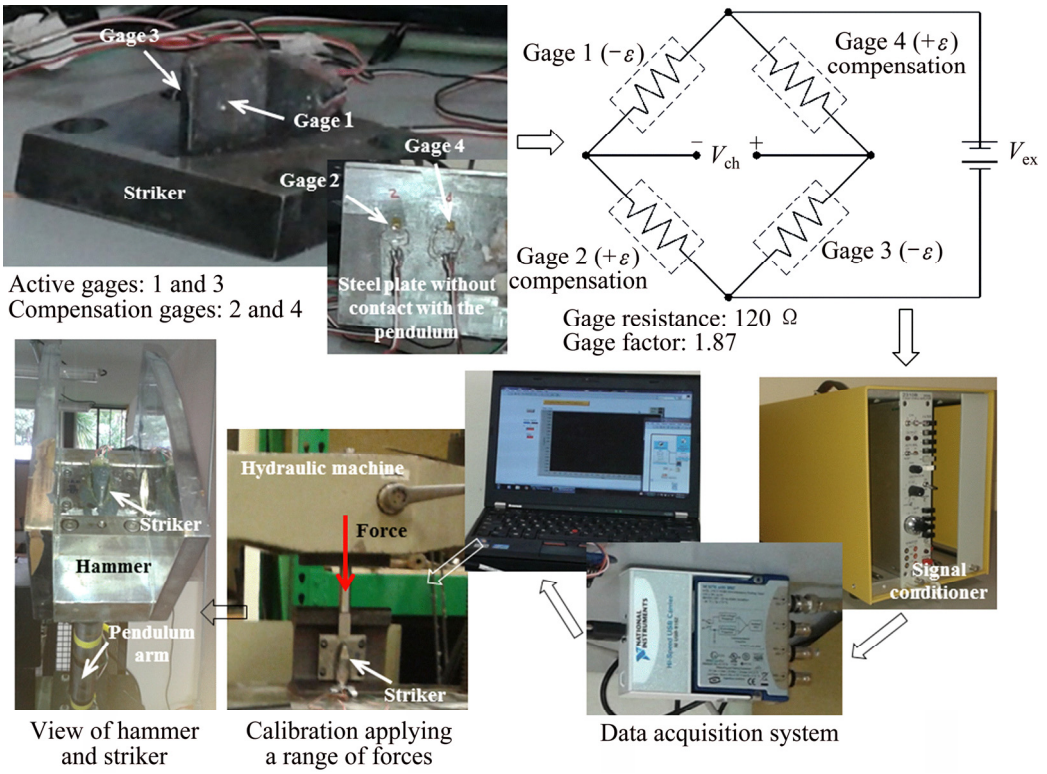

Fig. 4 Schematic diagram for instrumentation of striker

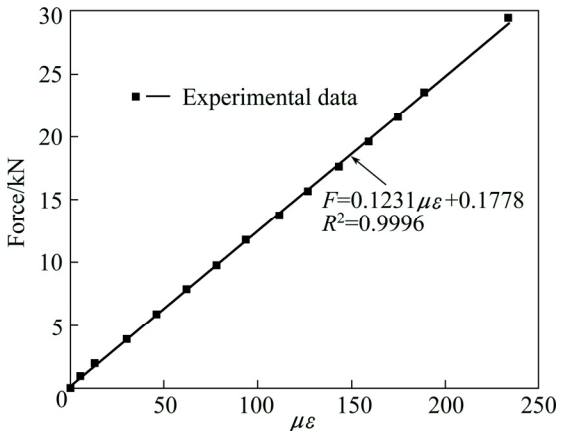

Fig. 5 Force−strain evolution of striker

samples machined from the base metal (Fig. 2). The maximum forces for the weld metal and the HAZ were 5 and 7.5 kN, which were roughly 50% and 25% lower than the maximum force for the base metal, respectively.

According to the representation of the force−time curve shown in Fig. 7, the yielding force F_{gy}, the force at the initiation of the crack F_{in}, the maximum force F_m, the force at the beginning of the unstable crack growth F_{iu}, and the force at the end of unstable crack growth F_a were calculated for the base metal (L and T designations), weld metal (W) and HAZ (Table 2).

To determine the crack initiation point, force−displacement curves for each material were plotted (Fig. 8). These curves represent the average values of four samples tested for each material (Fig. 6). The displacement was obtained by the following equation [13]:

$$s(t)=\int_{t_0}^{t}\left[v_0-\frac{1}{m}\int_{t_0}^{t}F(t)\mathrm{d}t\right]\mathrm{d}t \quad (2)$$

where $s(t)$ is the striker displacement, v_0 is the initial impact velocity, and m is the mass of the striker.

Subsequently, the compliance changing rate principle (CCR) [14] was used to identify a sudden transition point from the secant compliance gradient as indicated in Ref. [11]. Due to brittle behavior detected from the force−time curves in the base metal (longitudinal and transverse to rolling direction), certain values for F_{in} were not identified. In these cases, F_{in} were taken equal to F_m and F_{iu}.

Additionally, for each material and considering a constant impact velocity, the crack initiation energy E_{in}, the stable crack growth energy E_{stable}, the unstable crack growth energy $E_{unstable}$, and the fracture energy E_{all}, were determined using Eq. (1). These results are summarized in Table 3.

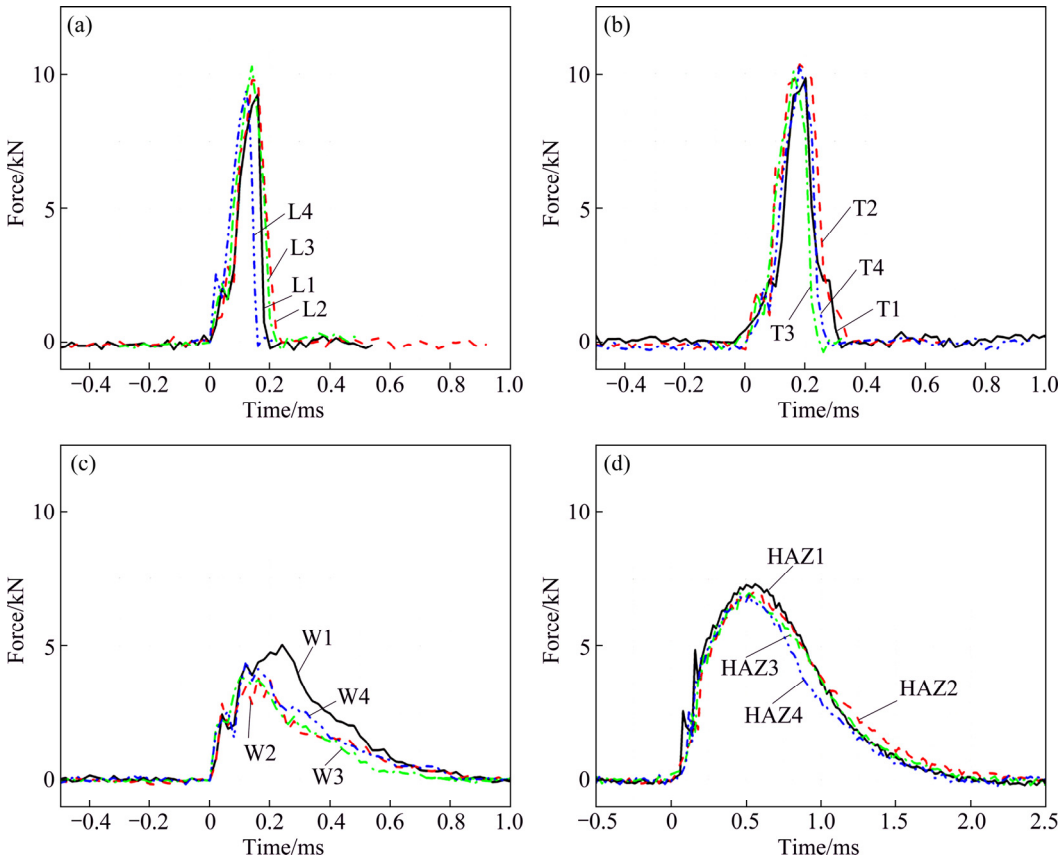

Fig. 6 Force−time evolution obtained from instrumented Charpy impact test for 7075-T651 aluminum alloy: (a) Longitudinal direction base metal; (b) Transverse direction base metal; (c) Weld metal; (d) Heat affected zone

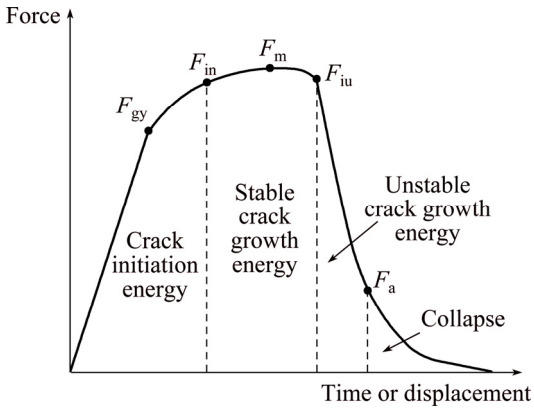

Fig. 7 Schematic representation for different stages of load as a function of time during impact test

Table 2 Results obtained from impact test for base metal (L and T), weld metal (W) and heat affected zone (HAZ)

Specimen	F_{gy}/kN	F_{in}/kN	F_m/kN	F_{iu}/kN	F_a/kN	Time to fracture/ms	$\int_{t=0}^{t=t_f} F(t)\mathrm{d}t$
L1	8.86	9.30	9.30	9.30	−	0.20	0.93
L2	7.87	9.80	9.80	9.80	−	0.24	1.29
L3	8.30	10.30	10.30	10.30	−	0.16	1.11
L4	9.13	9.30	9.30	9.30	−	0.22	0.77
Mean	8.54	9.67	9.67	9.67	−	0.20	1.02
S.D.	0.56	0.47	0.47	0.47	−	0.03	0.22
T1	9.21	9.36	9.83	9.83	3.00	0.32	1.41
T2	9.59	9.73	10.35	9.82	2.67	0.34	1.84
T3	8.37	10.08	10.08	10.08	2.50	0.26	1.14
T4	8.60	10.31	10.31	10.31	2.45	0.28	1.41
Mean	8.94	9.87	10.14	10.01	2.65	0.30	1.45
S.D.	0.55	0.41	0.23	0.23	0.24	0.03	0.28
W1	3.76	4.50	5.05	4.41	1.09	0.82	1.92
W2	2.99	3.44	3.82	2.98	1.53	0.84	1.31
W3	3.24	3.51	3.81	3.09	1.03	0.82	1.29
W4	3.50	3.67	4.41	3.66	1.04	0.82	1.50
Mean	3.37	3.78	4.27	3.53	1.17	0.82	1.50
S.D.	0.33	0.48	0.58	0.65	0.23	0.01	0.29
HAZ1	5.31	7.24	7.30	5.90	2.01	1.96	6.62
HAZ2	5.23	6.96	7.04	5.85	2.31	2.20	6.60
HAZ3	5.06	6.85	6.97	5.23	2.20	2.02	6.56
HAZ4	5.04	6.68	6.94	5.07	1.93	1.94	5.90
Mean	5.16	6.93	7.06	5.51	2.11	2.03	6.42
S.D.	0.13	0.23	0.16	0.42	0.17	0.11	0.34

From Table 3, it is observed that the crack initiation energy for the base metal does not have an important variation in terms of the rolling direction. However, the

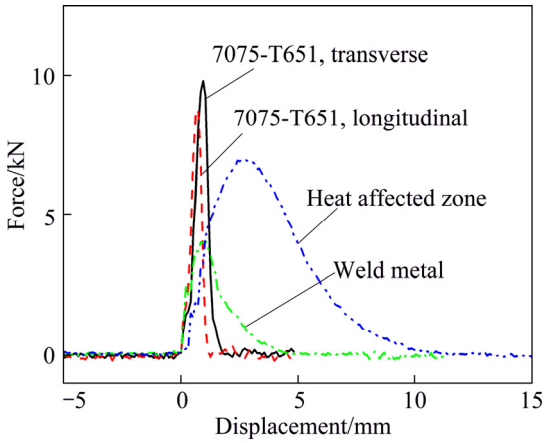

Fig. 8 Mean force−displacement curves obtained for 7075-T651 aluminum alloy (transverse and longitudinal to rolling direction), weld metal, and heat affected zone

Table 3 Energies at different stages during impact test

Specimen	E_{in}/J	E_{stable}/J	$E_{unstable}$/J	E_{all}/J
L1	4.11	−	−	4.86
L2	3.91	−	−	6.75
L3	3.47	−	−	5.83
L4	2.89	−	−	4.05
Mean	3.59	−	−	5.37
S.D.	0.54	−	−	1.17
T1	3.94	1.01	2.43	7.38
T2	4.47	3.18	1.98	9.63
T3	3.47	−	−	5.98
T4	4.50	−	−	7.37
Mean	4.09	2.09	2.20	7.59
S.D.	0.48	1.53	0.31	1.51
W1	2.88	2.47	4.70	10.05
W2	1.46	1.74	3.66	6.86
W3	2.50	2.16	2.10	6.76
W4	2.21	1.22	4.43	7.86
Mean	2.26	1.89	3.72	7.88
S.D.	0.60	0.54	1.16	1.52
HAZ1	13.13	9.33	12.24	34.70
HAZ2	9.95	11.00	13.65	34.60
HAZ3	12.64	9.55	12.17	34.36
HAZ4	10.65	9.76	10.36	30.77
Mean	11.59	9.91	12.10	33.60
S.D.	1.53	0.74	1.34	1.89

fracture energy in transverse direction is 40% higher than that in longitudinal direction. These results are in agreement with those previously reported in Refs. [8,15].

Despite the decrement of the maximum force during the impact test and the crack initiation energy for the weld metal and HAZ, fracture energy shows an increment with respect to the base metal. Regarding the

weld metal, fracture energy shows a marginal increment. However, for the HAZ, the time to fracture increases with respect to the base and weld metals. This aspect is attributed to the weld thermal cycle, which promotes an over-aging of the material due to the microstructural transformation of the fine hard and disperse η' precipitates to coarse precipitates. It means that a hardening decrement exists, because the microstructure in the HAZ exihbits the incoherent η phase ($MgZn_2$) precipitated in the α-aluminum matrix. As a consequence, the local ductility conditions of the soft zone in the HAZ tend to increase and the fracture energy of the HAZ (soft zone) increased in more than six times with respect to the base metal in longitudinal direction. It is to say that local mechanical properties play an important role in terms of toughness.

An approximation to the dynamic yield strength σ_{yd} for each condition of the material was determined by the following equation [16]:

$$\sigma_{yd} = \frac{2.99F_{gy}W}{B(W-a_0)^2} \quad (3)$$

where W and B are the width and thickness of the Charpy V-notch specimen, respectively. The crack length a_0, was taken as the initial notch.

Table 4 shows the results obtained for the dynamic yield strength and its respective comparison with those obtained for tensile test conditions (σ_y). It has been observed that σ_{yd} is lower than σ_y for all materials. This aspect is more evident for the base metal, where the ratio between σ_{yd}/σ_y is close to 0.72 and 0.78 for longitudinal and transverse directions, respectively. However, in the case of the weld metal and HAZ, this ratio tends to increase (0.96 for the weld metal and 0.89 for the HAZ). Although, the σ_{yd} determined by Eq. (3) is an approximation, the strain rate reached during the impact tends to decrease the yield strength in welds of a 7075-T651 aluminum alloy. This tendency is consistent with that reported previously in welds of a 6061-T6 aluminum alloy tested at middle strain rate [17], however, studies at different strain rates are needed to clarify this behavior.

Table 4 Yield strengths obtained from tensile (σ_y) and Charpy (σ_{yd}) tests

Material	σ_y/MPa	σ_{yd}/MPa
Base metal (longitudinal)	549	399
Base metal (transverse)	530	417
Weld metal	163	157
HAZ	270	241

The differences in the previously reported quantities (fracture energy, force applied during the impact tests and yield strength) among the base metal, weld metal and HAZ could be explained in view of the microstructural characteristics. The next section presents a fracture analysis for each material analyzed in this work.

3.2 Fracture characteristics

Figure 9 shows the fractured Charpy V-notch specimens for the base metal, weld metal and HAZ. The crack propagation for the base metal in longitudinal direction (Fig. 9(a)) was aligned to the normal impact force. However, in transverse direction, the crack propagation describes a zigzag pattern (Fig. 9(b)). In both cases, these characteristics were attributed to the granular structure morphology. The elongated grains produced by the high deformation of the material in longitudinal direction (Fig. 10(b)) increase the strength but decrease its ductility as previously been reported by ALATORRE et al [5]. This aspect promotes the propagation of the crack along grain boundaries following a straight path (brittle fracture). On the other hand, in transverse direction, the granular structure tends to be less elongated (Fig. 10(c)), i.e., there are more barriers to propagate the crack. This structure produces a propagation of the crack as a function of the grain morphology (intergranular propagation), and a certain

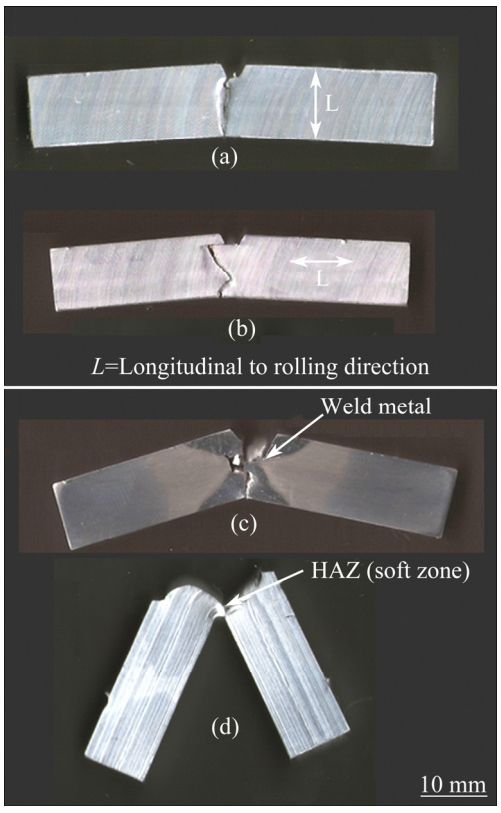

Fig. 9 Crack propagation in Charpy V-notch specimens: (a) Base metal in longitudinal direction; (b) Base metal in transverse direction; (c) Weld metal; (d) Heat affected zone

quantity of the impact energy is consumed during the plastic deformation.

For the weld metal specimens (Fig. 9(c)), the propagation of the crack presents a similar appearance to that of the base metal in transverse direction. In this case, the granular structure consists of dendrites with an equiaxed morphology in the center of the weld metal (Fig. 11). However, an interdendritic porosity produced during the solidification process due to the high solubility of the hydrogen in liquid aluminum was observed. This porosity causes an irregular crack propagation in the material, as well as low toughness (Table 3).

In contrast, for the HAZ (Fig. 9(d)), the crack describes a regular pattern, and a high level of deformation was observed. These characteristics were attributed to the fact that in the HAZ, the weld thermal cycle produces an over-aging phenomenon due to the transformation and coarsening of η' to η precipitates as reported in [6]. Thus, an important decrement of the hardening in the material is produced (Fig. 3), however, an increment in ductility is promoted due to the incoherence of the η phase with the aluminum α matrix.

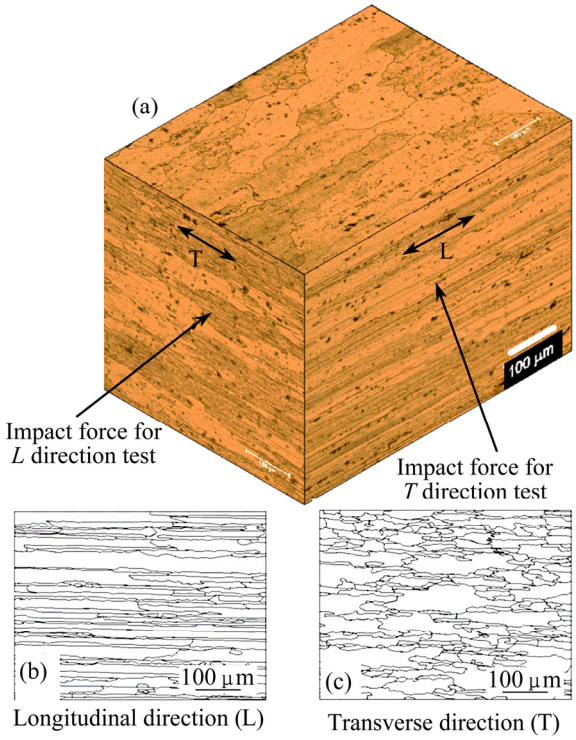

Fig. 10 Granular structures of 7075-T651 aluminum alloy (a), and longitudinal (b) and transverse (c) to rolling direction planes, respectively [5]

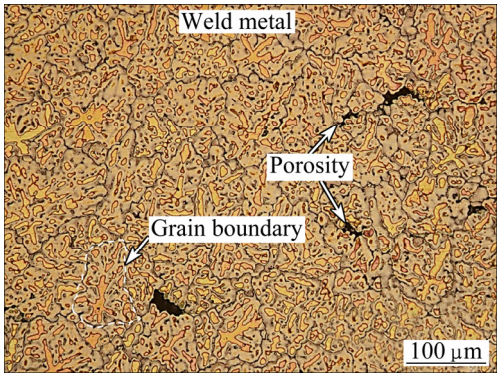

Fig. 11 Grain structure in center of weld metal [5]

Figure 12 shows a general view of the fracture appearance of the Charpy V-notch specimens for the base metal, weld metal and HAZ. A brittle fracture was observed for the base metal in both directions (Figs. 12(a) and (b)), characterized by a flat surface without lateral expansion. Though, for the fracture surfaces of the weld metal (Fig. 12(c)) and HAZ (Fig. 12(d)), the lateral expansion is more evident than that for the base metal. As a consequence, the fracture energy for the weld metal and HAZ is higher than that for the base metal (Table 3).

Figure 13 shows the fracture surfaces taken from a scanning electron microscope. Several crack initiation sites were observed for the longitudinal direction (Fig. 13(a)). These cracks were propagated along grain boundaries practically with no dimple formation, i.e., quasi-brittle fracture. However, for transverse direction (Fig. 13(b)), brittle fracture characteristics prevail with some ductile evidences reflected by fibrous zones, as well as the presence of some dimples. These features tend to slightly increase the ductility of the material, i.e., time to fracture increment shown in Fig. 6. As a consequence, an increment in the fracture energy was observed with respect to the base metal in longitudinal direction (Table 3).

In contrast, an evident ductile fracture was observed for the weld metal and HAZ (Figs. 13(c) and (d), respectively). These fracture surfaces are characterized by the nucleation, growth and coalescence of microvoids produced by the deformation process during the impact. For weld metal, the fracture surface (Fig. 13(c)) presents a high degree of porosity, which is produced by the high solubility of the hydrogen in liquid aluminum during the solidification process [18]. This aspect decreases the impact force and ductility of the material (Fig. 6(c)), however, the fracture energy tends to be higher than that of the base metal but lower than that of the HAZ (Table 3). For the HAZ, a fracture surface with a high level of ductility (dimples) in comparison with base metal was observed. The fracture energy for the HAZ increased in more than four times with respect to the base metal in transverse direction.

Further details of the fracture surfaces are presented in Fig. 14 at higher magnifications. An intergranular fracture was observed for the base metal in longitudinal direction (Fig. 14(a)). In metals, this fracture mechanism is typically related to intergranular corrosion, however, the precipitation of hard and brittle phases such as

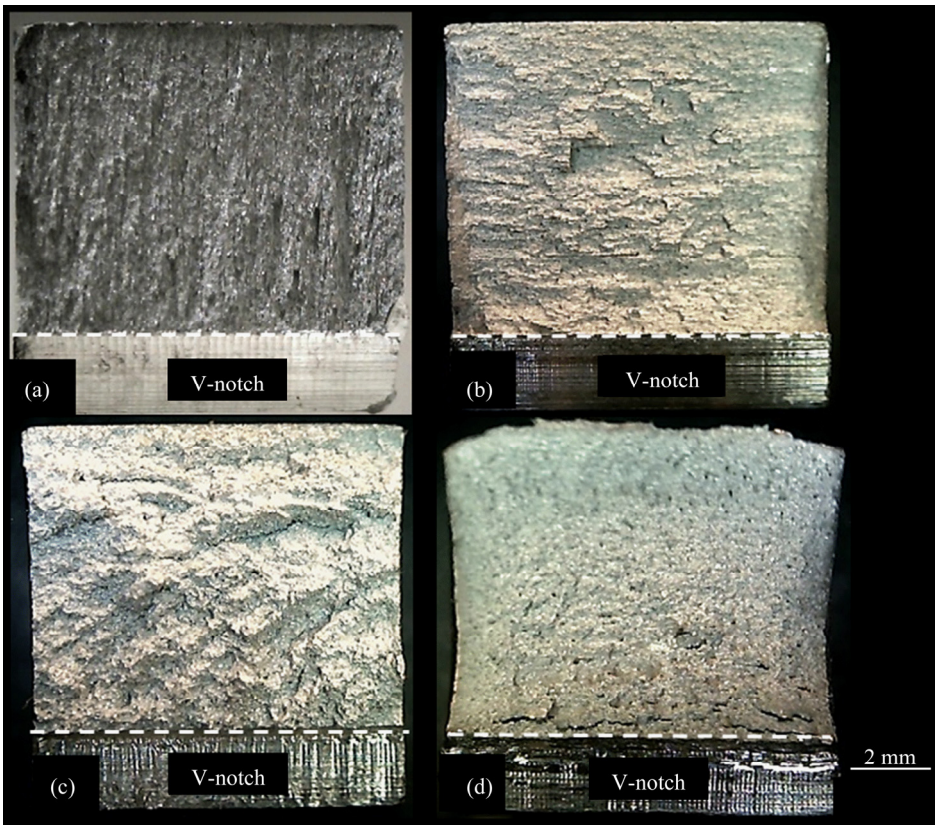

Fig. 12 General characteristics of fracture surfaces for base metal in longitudinal direction (a), base metal in transverse direction (b), weld metal (c) and heat affected zone (d)

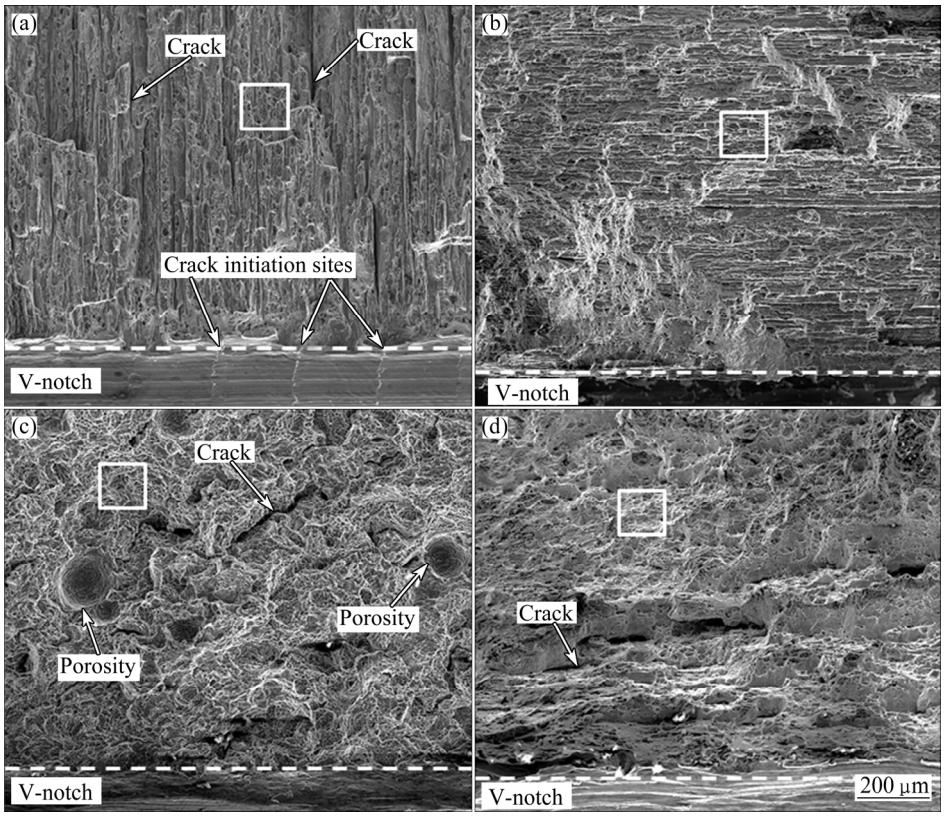

Fig. 13 Fracture surfaces for base metal in longitudinal direction (a), base metal in transverse direction (b), weld metal showing porosity formation (c) and heat affected zone (d)

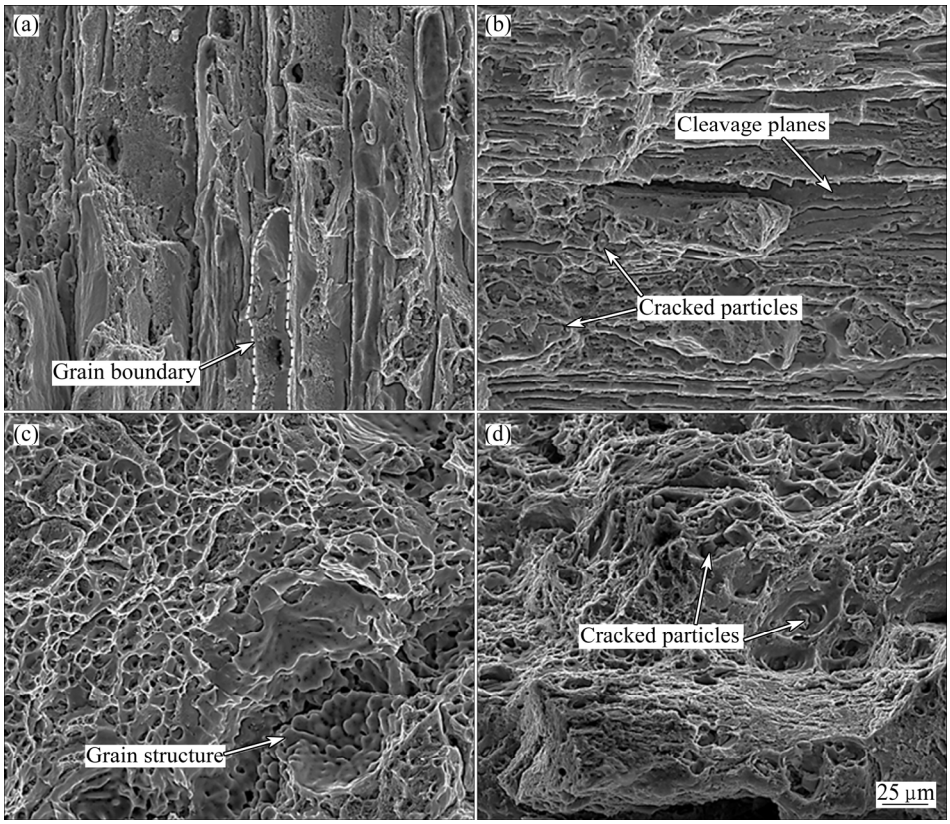

Fig. 14 Fracture surfaces details according to rectangles shown in Fig. 13

$MgZn_2$ on the grain boundary can produce an intergranular fracture [19]. In this case, the brittle phase is provided by the presence of η' precipitates (artificial aging T6) that increased the hardening of the material, but decreased the ductility. On the other hand, for the base metal in transverse direction, several cracked particles were observed and some micro-voids were nucleated, i.e., ductile failure. However, the high degree of deformation (cold rolling) in the alloy does not allow to continue with the ductile mechanism, instead the failure tends to follow a transgranular path, which is denoted by parallel cleavage planes (Fig. 14(b)).

On the contrary, the fracture surface for the weld metal (Fig. 14(c)) shows a mix of small ductile dimples between 5 and 10 μm in diameter. The fracture suggests that the crack nucleation is due to the presence of small empty holes (porosity) which leads to a loss of the impact-toughness and as a consequence the yield strength of the material.

On the other hand, the failure mechanism for the HAZ is attributed to the coarsening of the η' precipitates, which acts as points for the crack nucleation and coalescence of the microvoids, as can be seen in Fig. 14(d).

4 Conclusions

1) According to the force versus time curves, the base metal exhibited a brittle behavior in the longitudinal and transverse directions, while the weld metal and the HAZ presented a ductile behavior.

2) The maximum forces applied during the impact tests were 4.27 and 6.93 kN for the weld metal and the HAZ, respectively. These values were lower than the corresponding ones for the base metal in the longitudinal and transverse to rolling direction (9.67 and 10.31 kN). Regarding the time required to fracture the Charpy V-notch specimens, the lower values were for the base metal (0.2 ms for the longitudinal direction and 0.3 ms for the transverse direction). Meanwhile, the time increased considerably for the weld metal (0.82 ms) and the HAZ (2.03 ms).

3) The fracture energy was 33.6 J for the HAZ, 7.88 J for the weld metal, 5.37 J for the base metal in the longitudinal direction and 7.37 J for the transverse direction. The microstructural transformation from fine and hard η' precipitates to coarse η precipitates promoted the toughness in the HAZ. This microstructural transformation caused a considerably increase of the fracture energy for the HAZ with respect to the base metal value. The fracture energy for the weld metal was higher than that for the base metal because of the pore formation during solidification.

4) The fracture surfaces revealed that the base metal in longitudinal direction presented an intergranular failure, whereas, for the transverse direction, the failure

was predominately brittle (cleaveage) with some insights of ductile characteristics (dimples). Finally, a ductile failure was observed for the weld metal and the HAZ due to the nucleation, growth and coalescence of microvoids during the impact test.

5) The results of this research suggest that the microstructural evolution produced by the welding procedure could be tailored by means of artificial cooling, in order to achieve a better compromise of properties (ductile−brittle behavior).

Acknowledgements

The authors thank to CONACyT (project CB 177834) and SIP-IPN for the funds given to conduct this research.

References

[1] ASTM. B209. Standard specification for aluminum and aluminum-alloy sheet and plate, in aluminum and magnesium alloys [S].

[2] HU B, RICHARDSON I M. Microstructure and mechanical properties of AA7075(T6) hybrid laser/GMA welds [J]. Materials Science and Engineering A, 2007, 459: 94−100.

[3] FULLER C B, MAHONEY M W, CALABRESE M, MICONA L. Evolution of microstructure and mechanical properties in naturally aged 7050 and 7075 Al friction stir welds [J]. Materials Science and Engineering A, 2010, 527: 2233−2240.

[4] ROBSON J D, UPADHYAY P, REYNOLDS A P. Modelling microstructural evolution during multiple pass friction stir welding [J]. Science and Technology of Wedling and Joining, 2010, 15(7): 613−618.

[5] ALATORRE N, AMBRIZ R R, NOUREDDINE B, AMROUCHE A, TALHA A, JARAMILLO D. Tensile properties and fusion zone hardening for GMAW and MIEA welds of a 7075-T651 aluminum alloy [J]. Acta Metallurgica Sinica, 2014, 27(4): 694−704.

[6] HWANG R Y, CHOU C P. The study on microstructural and mechanical properties of weld heat affected zone of 7075-T6 aluminum alloy [J]. Scripta Materialia, 1998, 38(2): 215−221.

[7] RINGER S P, HONO K. Microstructural evolution and age hardening in aluminium alloys: Atom probe field-ion microscopy and transmission electron microscopy studies [J]. Materials Characterization, 2000, 44: 101−131.

[8] TAJALLY M, HUDA Z, MASJUKI H H. A comparative analysis of tensile and impact-toughness behavior of cold-worked and annealed 7075 aluminum alloy [J]. International Journal of Impact Engineering, 2010, 37: 425−432.

[9] CHEN Y, PEDERSEN K O, CLAUSENA A H, HOPPERSTADA O S. An experimental study on the dynamic fracture of extruded AA6xxx and AA7xxx aluminium alloys [J]. Materials Science and Engineering A, 2009, 523: 253−262.

[10] SAHRAOUI S, LATAILLADE J L. Analysis of load oscillations in instrumented impact testing [J]. Engineering Fracture Mechanics, 1998, 60(4): 437−446.

[11] ALEXOPOULOS N D, STYLIANOS A, CAMPBELL J. Dynamic fracture toughness of Al−7Si−Mg (A357) aluminum alloy [J]. Mechanics of Materials, 2013, 58: 55−68.

[12] SERVER W L, WULLAERT R A, SHECKHERD J W. Evaluation of current procedures for dynamic fracture-toughness testing [J]. American Society for Testing and Materials, 1977, 631: 446−461.

[13] LANDREIN P, LORRIOT T, GUILLAUMAT L. Influence of some test parameters on specimen loading determination methods in instrumented Charpy impact tests [J]. Engineering Fracture Mechanics, 2001, 68: 1631−1645.

[14] KOBAYASHI T. On the information about fracture characteristics obtained from instrumented impact test of A533 steel for reactor pressure vessel [J]. Engineering Fracture Mechanics, 1984, 19(1): 67−69.

[15] CEPEDA-JIMENEZ C M, RUANO O A, CARREÑO F. Fracture mechanisms assessment of a multilayer material with high strength and excellent impact toughness based on the aerospace Al 7075 alloy [J]. Revista de Metalurgia, 2012, 48(4): 290−302.

[16] SERVER L. General yielding of Charpy V-notch and precracked Charpy specimens [J]. Journal of Engineering Materials and Technology, 1978, 100(2): 183−188.

[17] AMBRIZ R R, FROUSTEY C, MESMACQUE G. Determination of the tensile behavior at middle strain rate of AA6061-T6 aluminum alloy welds [J]. International Journal of Impact Engineering, 2013, 60: 107−119.

[18] HATCH J E. Aluminum: Properties and physical metallurgy [M]. Ohio: ASM International, 1984.

[19] KUMAR P V, REDDY G M, RAO K S. Microstructure, mechanical and corrosion behavior of high strength AA7075 aluminium alloy friction stir welds—Effect of post weld heat treatment [J]. Defence Technology, 2015, 11(4): 362−369.

采用改进冲击摆锤评价 7075-T651 合金焊缝的断裂能

R. R. AMBRIZ[1], D. JARAMILLO[1], C. GARCÍA[2], F. F. CURIEL[3]

1. Instituto Politécnico Nacional CIITEC-IPN, Cerrada de Cecati S/N Col. Sta. Catarina C.P 02250, Azcapotzalco, DF, México;

2. Mechanical and Aerospace Engineering, Carleton University, 1125 Colonel By Drive, Ottawa, ON, K1S 5B6, Canada;

3. Universidad Autónoma de Coahuila (UAdeC), Facultad de Metalurgia, Carr. 57, Km 5, Monclova, Coahuila, México

摘　要：采用改进冲击摆锤，研究 7075-T651 合金焊缝夏比试样的力−时间曲线。考虑力−时间曲线和恒冲击速率，获得不同区域的断裂能。与焊缝金属(7.88 J)和基体金属(5.37 J(纵向)和 7.37 J(横向))的断裂能相比，热影响区的断裂能更高(33.6 J)，这是由于焊接过程中，热力学不稳定的 η'相发生组织转变。焊缝区的断裂能比基体合金的高，这是由于焊接凝固过程中产生大量孔洞。为从力−时间曲线中获得动态屈服力，对焊缝、热影响区和基体合金的屈服强度进行近似处理。断裂形貌表明，基体合金在纵向方向上呈现晶间断裂，而在横向方向上，主要为脆性(解理)断裂并伴有韧性断裂特征。而焊缝区和热影响区则呈现韧性断裂。

关键词：7075-T651 焊接接头；改进夏比摆锤；力−时间曲线；断裂能；动态屈服强度

(Edited by Yun-bin HE)